THERMODYNAMICS 2019 SPECIAL ISSUE

Dynamics of polydisperse hard-spheres under strong confinement

Ryan C. Roberts, Nico Marioni, Jeremy C. Palmer, and Jacinta C. Conrad

Department of Chemical and Biomolecular Engineering, University of Houston, Houston, TX, USA

ARTICLE HISTORY
Compiled January 31, 2020

ABSTRACT
We use molecular simulation to probe the connection between local structure and the unusual re-entrant dynamics observed for polydisperse hard-sphere liquids confined in thin slit pores. The local structure is characterized by calculating 2-D bond-orientational order parameters associated with square and hexatic order for particles in the layer adjacent to the confining walls. When the wall separation is commensurate with the average particle size, the particles primarily exhibit local hexatic order, whereas local square order increases in prevalence for incommensurate geometries. The relaxation time extracted from the ensemble-averaged mean-square displacement increases exponentially with the static correlation length associated with hexatic local order in strongly confined commensurate geometries, in agreement with theoretical predictions for dynamical slowing. Square order, by contrast, is not associated with a growing length scale for either commensurate or incommensurate geometries, indicating that it is strongly geometrically frustrated. Our results suggest that the influence of bond-orientational order on dynamical slowing may be altered by changing the extent of confinement.

KEYWORDS
Glass transition; molecular dynamics; confinement; hard spheres; correlation length

1. Introduction

The underlying mechanisms responsible for the dramatic slowing of dynamics by many orders of magnitude upon compression or cooling of dense liquids are incompletely understood and intensely debated [1, 2]. Near the glass transition, particles are trapped in long-lived cages formed by their neighbors, and are able to relax only when the cages rearrange. Phenomenologically, this relaxation is viewed as a two-step process involving movement within and escape from the cage formed by the neighbors [3–5]. This coupling to neighbor configuration suggests that the surrounding structure is a strong determinant of glassy dynamics. How the nature of the cages and their relaxations depend on the structure of the liquid remain open questions. The length scale and structural motifs associated with these relaxations are thought to be non-local [6, 7]. Indeed, upon cooling or compressing the dynamics of liquids become increasingly heterogeneous in space and time. These spatial heterogeneities are thought to be connected to a growing length scale over which dynamics are correlated [8–10].

CONTACT Jeremy Palmer jcpalmer@uh.edu
CONTACT Jacinta Conrad jcconrad@uh.edu

Confining a liquids inside a thin geometry modifies the dynamics and introduces a competing length scale H, characterizing the extent of confinement. [11–14]. For hard-sphere fluids under weak confinement ($H \gtrsim 5$ particle diameters) the dynamics slow monotonically as the confinement length scale is decreased [14, 15]. In strongly-confined hard-sphere systems ($H \lesssim 5$ particle diameters), by contrast, the relaxation times can depend non-monotonically on the separation between the walls [15–20]. At high particle densities, this non-monotonic behavior can lead to multiple glass transitions [17], as predicted by mode-coupling theory [16]. Notably, the glass transition line for polydisperse hard spheres exhibits oscillations whose period is of the order of the particle diameter [17], strongly intimating that the competition between layering and local packing drives the unusual dynamical re-entrance observed in these systems.

For certain glass-forming systems, bond-orientational order has been shown to be connected to dynamics. Numerical simulations of 2-D polydisperse hard disks, for example, reveal that transient clusters of highly-ordered particles are correlated with dynamical heterogeneity [21]. In several systems, the clusters associated with such medium-range crystalline order (MRCO) are hexatically-ordered in 2-D [22, 23] or hexagonally-ordered in 3-D [24–26]. Whereas the static and dynamic length scales have been shown to grow similarly for 2-D glasses with MRCO, this behavior is not observed in other 2-D glass formers [27, 28]. In strongly confined systems, MRCO is enhanced within the layers of particles that form near the confining walls [29]. When the confinement length scale is commensurate with particle size, particles within the layers typically adopt hexatic order parallel to the walls. By contrast, incommensurate geometries tend to promote square ordering [30–32]. While these earlier studies show that MRCO is amplified by strong confinement, they have not explored its link to dynamics.

In this study, we use molecular dynamics (MD) simulations to investigate the connection between local structural ordering and the unusual re-entrant dynamics observed for polydisperse hard-sphere liquids confined in small slit pores. Despite the polydisperse nature of these systems, the particles in the contact layers adjacent to the confining walls exhibit pronounced local ordering, whose symmetry changes as the wall separation becomes incommensurate with the average particle size. Particles in commensurate geometries largely exhibit hexatic local order, whereas square local order is also observed in systems where the confinement length scale is incommensurate with particle size. The static correlation length associated with hexatic local order is found to increase logarithmically with the relaxation time, in agreement with predictions from 2-D random first-order theory [33] and models based on locally-favored structures [34]. Square ordering, by contrast, is short-ranged and not associated with a growing length scale even for incommensurately-packed systems in which square ordering is most prevalent. This observation suggests that square order is strongly geometrically frustrated for all levels of confinement studied here. For incommensurate geometries, neither hexatic nor square ordering are associated with a growing length scale. This striking result indicates that the connection between bond-orientational order and dynamical slowing can be altered by varying confinement.

2. Methods

Event-driven MD simulations were performed to investigate the behavior of polydisperse hard-spheres confined in slit-shaped pores consisting of two parallel walls separated by distance H along the z-axis of the cell. Periodic boundary conditions

were imposed along the x- and y-axes parallel to the walls to model an infinite slab geometry. Each of the $N = 10976$ particles in the system was assigned unit mass and a hard-core diameter σ_i randomly sampled from a Gaussian distribution. The average of the distribution was set to $\bar{\sigma} = 1$ and the standard deviation s was chosen to modulate particle polydispersity (PDI). Following convention, we adopt units in which Boltzmann's constant $k_{\mathrm{B}} = 1$, and $\bar{\sigma}$ and $t = \bar{\sigma}(m/k_{\mathrm{B}}T)^{1/2}$ are the fundamental measures of length and time, respectively [17, 35]. All simulations were performed in the microcanonical (NVE) ensemble, with initial particle momenta randomly drawn from the Maxwell-Boltzmann distribution with specified temperature $T = 1$.

We investigated the static and dynamic properties of the confined hard-spheres at various state points specified by $\{s, \phi, H\}$, where ϕ is the particle volume fraction. For PDI $s = 0.15$, we examined ranges $0.47 \leq \phi \leq 0.51$ and $2.00 \leq H \leq 3.00$. For $s = 0.05$, we considered $2.00 \leq H \leq 3.00$ at a single volume fraction $\phi = 0.51$. The systems were prepared by incrementally compressing an initial confined liquid-like configuration at $\phi = 0.45$ to achieve the final H and ϕ. The compression steps were performed in increments of $\Delta\phi = 0.01$, following each step by a short MD simulation ($10t$) at constant ϕ to relax compression-induced stresses. After compression, the systems were equilibrated until their properties became invariant with sample age. The sample age was measured as the waiting time t_w, defined as the time elapsed since the end of the final compression step.

For all systems, we computed the mean 2-D Mermin order parameters averaged over particles in the wall contact layers [36]

$$\psi_l = \frac{1}{N_{\mathrm{wall}}} \sum_{j=1}^{N_{\mathrm{wall}}} \psi_l^j \tag{1}$$

where

$$\psi_l^j = \frac{1}{n_j} \sum_{k=1}^{n_j} e^{il\theta_{jk}}, \tag{2}$$

N_{wall} is the number of particles in the wall contact layers, n_j is the number of nearest neighbors of particle j, $i = \sqrt{-1}$, l is a positive integer indicating the orientational symmetry, $\theta_{jk} = \cos^{-1}\left[\hat{\mathbf{i}} \cdot \mathbf{r}_{jk} |\mathbf{r}_{jk}|^{-1}\right]$ is the angle between the x-axis and the in-plane interparticle separation vector $\mathbf{r}_{jk} = \mathbf{r}_j - \mathbf{r}_k$, $\hat{\mathbf{i}}$ is the unit vector along the x-axis, and $\mathbf{r}_j = \{x_j, y_j\}$ is the in-plane particle position vector for particle j. The contact layers were identified by computing the density profile along the z-axis perpendicular to the walls

$$\rho(z) = \frac{1}{N\Delta z} \sum_{j=1}^{N} \delta(z - z_j), \tag{3}$$

where z_j is the out-of-plane particle coordinate and Δz is the bin width. Particles with z-coordinates lying between the first two minima in $\rho(z)$ nearest to each wall were defined as belonging to the contact layers. Equation 2 was evaluated by taking the sum over the nearest neighbors of the central particle j that lie within the same layer and a cutoff separation distance of $r = 1.34$, which approximately encompasses the first coordination shell.

We monitored ψ_4 and ψ_6, which are sensitive to square and hexatic ordering, respectively. The order parameter $\psi_4 = 1$ for perfect long-range square ordering, whereas $\psi_6 = 1$ for systems with perfect long-range hexatic ordering. For disordered systems, $\psi_4 \to 0$ and $\psi_6 \to 0$ as $N \to \infty$, but they take on small positive values near zero in finite systems due to fluctuations. Systems with appreciable square and/or hexatic ordering (i.e., $\psi_4 \geq 0.05$ and/or $\psi_6 \geq 0.05$) were considered equilibrated when the Mermin order parameters became invariant with sample age (within statistical uncertainty). This invariance was observed for t_w ranging from 20000 – 100000. For the remaining (disordered) systems, equilibration was monitored by computing the the pore-averaged mean-square displacement (MSD)

$$\Delta r^2(t) = \frac{1}{N}\sum_{k=1}^{N}(\mathbf{r}_k^2(t) - \mathbf{r}_k^2(0))^2 \tag{4}$$

as a function of sample age. The systems were considered equilibrated when the MSDs computed over different time periods became statistically invariant with respect to sample age. This criterion was met for t_w ranging from 200 – 30000 simulation time units, depending on the state conditions.

Following equilibration, the simulations were extended to generate a production phase, during which trajectories were saved for subsequent analysis. The duration of the production phase was typically a factor of 10 longer than the equilibration period. Statistical properties at each state point were computed by averaging over $N_\mathrm{s} = 5, 10,$ or 20 independent simulations, depending on the PDI, each initiated from a different particle configuration prepared using the procedures described above.

The correlation lengths ξ_l associated with l-fold symmetry were estimated by computing the in-plane spatial correlation functions for the 2-D Mermin parameters

$$g_l(r) = \frac{L^2}{2\pi r \Delta r N_\mathrm{wall}(N_\mathrm{wall}-1)}\sum_{j\neq k}\delta(r - |\mathbf{r}_{jk}|)\psi_l^j\psi_l^{k*} \tag{5}$$

where L is the length of the simulation cell in the direction parallel to the walls, Δr is the histogram bin width, and $\psi_l^j\psi_l^{k*} = \mathrm{Re}\,(\psi_l^j)\mathrm{Re}\,(\psi_l^k) + \mathrm{Im}\,(\psi_l^j)\mathrm{Im}\,(\psi_l^k)$. Equation 5 was evaluated for $l = 4, 6$ to analyze the extent of square and hexatic ordering in the contact layers, respectively. The correlation lengths for both symmetries were extracted by fitting an exponential

$$f(r) = A\exp\left[-2r/\xi_l\right] \tag{6}$$

to the envelope of $g_l(r)/g(r)$, where $g(r)$ is the in-plane radial distribution function computed by evaluating Eq. 5 with the product $\psi_l^j\psi_l^{k*}$ omitted [37, 38]. An exponential fitting function was used because the usual Ornstein-Zernike (OZ) expression, which predicts power-law decay r^{-n}, is derived for isotropic systems, whereas the confined systems studied here are anisotropic [39].

To characterize the relaxation dynamics, we calculated $S_{00}^{(s)}(q,t)$, which is the self-part of the first component of the matrix

$$S_{\mu\nu}(q,t) = \frac{1}{N}\langle\rho_\mu(\mathbf{q},t)^*\rho_\nu(\mathbf{q},0)\rangle \tag{7}$$

indexed by non-negative integers μ, ν. Equation 7 is a generalization of the intermediate scattering function to systems confined in one dimension, with associated density fluctuations

$$\rho_\mu(\mathbf{q}, t) = \sum_{j=1}^{N} \exp\left[iQ_\mu z_j(t)\right] e^{i\mathbf{q}\cdot\mathbf{r}_j(t)}. \tag{8}$$

Here, $\mathbf{q} = \{q_x, q_y\}$ is the wavevector with norm q, $Q_\mu = 2\pi\mu H^{-1}$ is a discrete wavenumber, and $\mathbf{r}_j = \{x_j, y_j\}$ and z_j are the in- and out-of-plane particle coordinates, respectively.

3. Results and Discussion

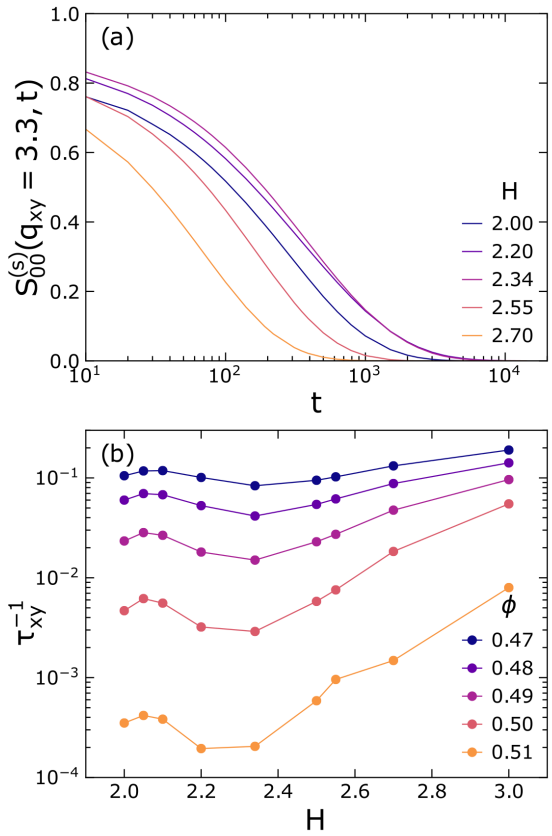

Figure 1. (a) Pore-averaged self-intermediate scattering functions $S_{00}^{(s)}(q_{xy}\bar{\sigma} = 3.3, t)$ in the direction parallel to the confining walls for a system with $\{s, \phi\} = \{0.15, 0.50\}$ for different wall separations H. (b) Inverse relaxation time τ_{xy}^{-1} in the direction parallel to the walls as a function of H for systems with $s = 0.15$ and different volume fractions ϕ. The relaxation times are defined via $S_{00}^{(s)}(q_{xy}\bar{\sigma} = 3.3, \tau_{xy}) = 1/e$.

We first examine the dynamics of strongly confined liquids parallel to the direction of confinement through the intermediate scattering function $S_{00}^{(s)}(q_{xy}\bar{\sigma} = 3.3, t)$ at the wave-vector corresponding to a length scale of approximately two particle diameters (Fig. 1(a)). For wall separations $2 \leq H \leq 3$, $S_{00}^{(s)}(q_{xy}\bar{\sigma} = 3.3, t)$ fully decays to zero on

time scales accessible with simulation. We define the in-plane, pore-averaged relaxation time scale τ_{xy} via $S_{00}^{(s)}(q_{xy}\bar{\sigma} = 3.3, \tau_{xy}) = 1/e$. The out-of-plane dynamics also fully relax, but the terminal relaxations are not diffusive due to the confinement imposed along the this direction and thus are not discussed further.

The in-plane relaxation dynamics depend non-monotonically on the wall separation H (Fig. 1(b)). At a volume fraction of $\phi = 0.47$, the inverse relaxation time τ_{xy}^{-1} depends only weakly on H. Near $H \approx 2.1$, τ_{xy}^{-1} exhibits a weak local maximum, and near $H \approx 2.3$ it exhibits a modest local minimum. Thus, highly confined, disperse suspensions exhibit re-entrant dynamics. These local extrema become more pronounced as ϕ is increased to 0.51. Our results are qualitatively similar to those of Ref. [17], which reported re-entrant diffusivities, extracted from the long-time limit of the ensemble-averaged mean-square displacements, for strongly confined suspensions of polydisperse hard spheres.

To gain insight into the changes in the underlying microstructure that are responsible for these unusual re-entrant dynamics, we first examine the number density profiles along the direction perpendicular to the walls, $\rho(z)$. The evolution of $\rho(z)$ with increasing ϕ varies markedly with the wall separation H. For $H = 2.20$, $\rho(z)$ does not strongly depend upon ϕ (Fig. 2(a)). Two layers form near the walls in all systems, and $\rho(z)$ is slightly enhanced near the pore center at $z = 0$ as ϕ is increased. Increasing the wall separation slightly to $H = 2.34$ leads to a stronger enhancement in density near the pore center with increasing ϕ (Fig. 2(b)). Systems confined at $H = 2.50$, however, show pronounced variation in $\rho(z)$ with ϕ (Fig. 2(c)). Three layers form in these systems. Further, as ϕ is increased the local maxima and minima respectively increase and decrease in height, indicating that layering becomes more pronounced. An additional increase in the wall separation, to $H = 3.00$, reveals three layers whose density profiles do not strongly vary with ϕ (Fig. 2(d)), as for $H = 2.00$.

The evolution in $\rho(z)$ with H indicates a change in the ordering of particle layers within the pore. For commensurate wall separations H, the ratio $H/\bar{\sigma}$ takes integer values and particles organize into close-packed layers [31, 40]. Incommensurate wall separations are those for which $H/\bar{\sigma}$ takes on non-integer values, disrupting the close-packed layers. For our systems, the development of incommensurate packing (between $H = 2.20$ and $H = 2.34$, Fig. 2(a,b)) coincides with the minimum in τ_{xy}^{-1} (Fig. 1). The development of incommensurate packing was observed to correlate with slow dynamics and larger nonergodicity parameters in Ref. 41, suggesting that motion in the confining plane is obstructed by such packings. For $H = 2.20$, however, relaxation times increase markedly without the formation of incommensurate layers, suggesting additional mechanisms for dynamical slowing.

To explore other mechanisms leading to dynamical slowing, we examine the local structure of particles in layers. Previous studies of monodispersed particles [30–32, 42] have shown that fully developed incommensurate packings for nearly half-integer values of $H/\bar{\sigma}$ are accompanied by a change in the in-plane local crystal structure. In monodisperse systems, increasing the wall separation from 2 to 3 particle diameters at $\phi \approx 0.50$ drives a transition in the in-plane order from $2\triangle \rightarrow 3\square \rightarrow 3\triangle$, where $\triangle$ and $\square$ indicate hexatic and square order, and the integers indicate the number of distinct particle layers [32]. Although our systems are polydisperse, we hypothesize that the change in commensurability in our system is also accompanied by a change in the the local structure of the particles.

To scrutinize the evolution of local structure in our systems, we calculate ψ_4^j and ψ_6^j (Eq. 2) for particles within the layers nearest to the wall (Fig. 3(a)). The parameters ψ_4^j

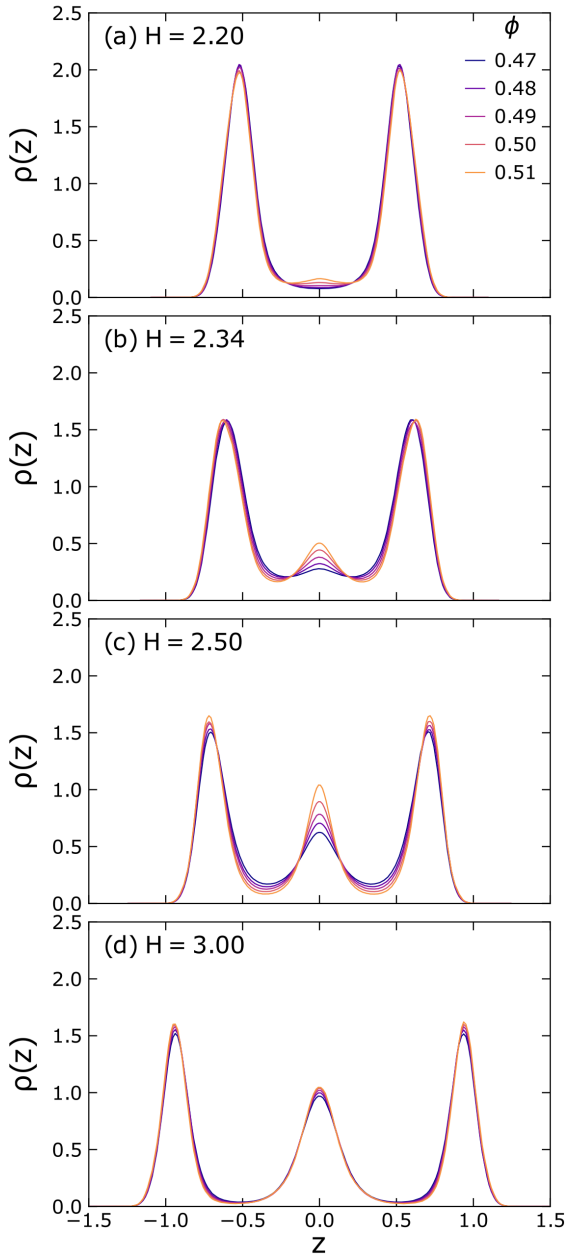

Figure 2. Number density profiles $\rho(z)$ in the direction perpendicular to the confining walls for (a) $H = 2.20$, (b) $H = 2.34$, (c) $H = 2.50$, and (d) $H = 3.00$ and volume fractions ϕ denoted in the legend. Each system has a polydispersity of $s = 0.15$.

and ψ_6^j are local variants of the spatially averaged 2-D Mermin parameters (Eq. 1) that characterize the extent of square and hexatic order in the coordination environments of individual particles, respectively. We first examine a low-dispersity system (PDI 5%, $s = 0.05$) with $\phi = 0.51$, whose structure is expected to closely mimic that of confined monodisperse spheres. The phase behavior of unconfined bulk systems was found to be qualitatively similar to the monodisperse limit below a threshold particle polydispersity [43, 44]. This threshold is larger for confined than unconfined particles [17, 35]. In our confined systems, increasing the wall separation from $H = 2.20$ to 3.00

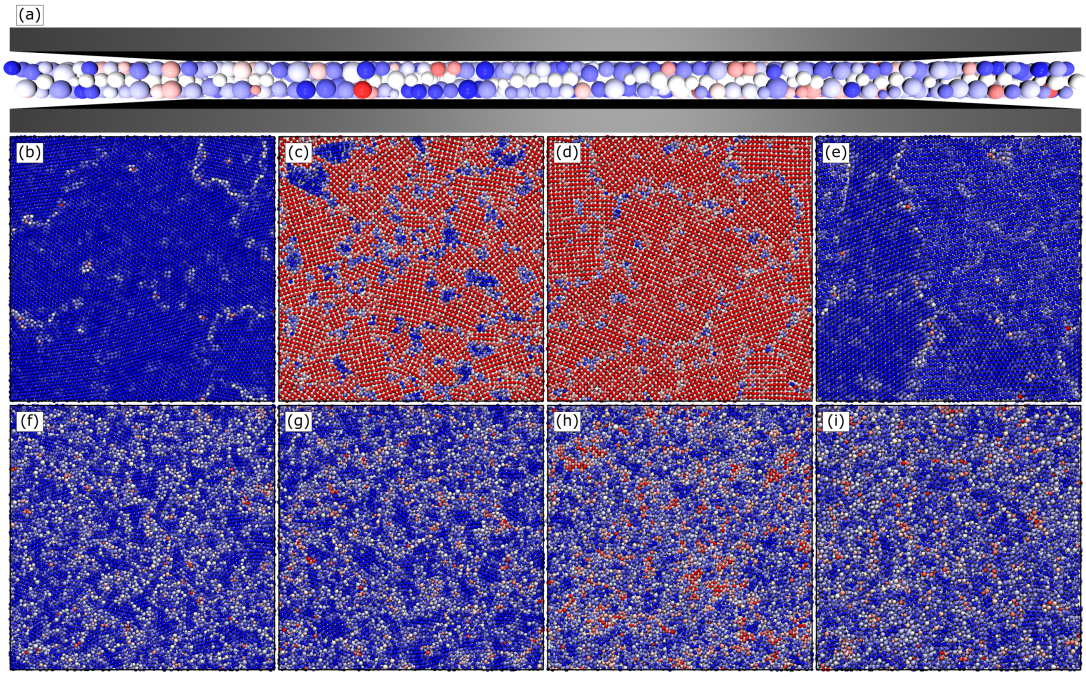

Figure 3. Renderings of systems with a particle volume fraction of $\phi = 0.51$ in the direction parallel (a) and perpendicular (b-i) to the confining walls. Particles within the contact layers adjacent to the walls are colored according to the magnitudes of the local Mermin order parameters (Eq. 2) with dark blue and dark red indicating $\psi_6 = 1$ and $\psi_4 = 1$, respectively. Particles with $\psi_6 \approx \psi_4 \approx 0$, or not within the wall contact layers, are colored white. (a) Rendering of system with $\{s, \phi, H\} = \{0.15, 0.51, 2.50\}$ in the direction parallel to the confining walls. The walls are depicted as gray slabs. Renderings in the direction perpendicular to the walls (b-e) are for systems with $\{s, \phi\} = \{0.05, 0.51\}$ and (b) $H = 2.20$, (c) $H = 2.34$, (d) $H = 2.50$, and (e) $H = 3.00$. Renderings (f-i) are for systems with $\{s, \phi\} = \{0.15, 0.51\}$ and (f) $H = 2.20$, (g) $H = 2.34$, (h) $H = 2.50$, and (i) $H = 3.00$

leads to changes in the predominant local order in the wall contact layers (Fig. 3(b-e)). For $H = 2.20$ particles primarily exhibit hexatic local order. For $H = 2.34$ local hexatic and square order coexist, whereas for $H = 2.50$ local square order is dominant. Finally, at $H = 3.00$ the particles near the wall again exhibit primarily hexatic local order. These observations indicate that the extent of hexatic local ordering is re-entrant. Hexatic local order is more prevalent in strongly confined systems for which packing is commensurate. Square ordering becomes more prevalent in incommensurate packings as a mechanism by which particles resolve frustration in ordering, forming BCC-like local arrangements in the direction perpendicular to the pore walls.

The transition from hexatic to square local order observed in our simulations with $s = 0.05$ is consistent with the $2\triangle \rightarrow 3\square$ transition observed for monodisperse hard spheres over this range of wall separations [32]. Further, the coexistence of square and hexatic motifs in $H = 2.34$ is analogous to two-phase coexistence between $2\triangle$ and $3\square$ observed from the free energy calculations of Ref. [32]. Indeed, despite the modest dispersity, all systems with $s = 0.05$ fully crystallize on the simulated time scales.

Re-entrance in the extent of hexatic order is also observed with increasing wall separation when the dispersity is increased to 15% (Fig. 3(f-i)). The fraction of particles with locally square order increases as H is increased from 2.00 to 2.50, and then decreases for larger wall separations. The size of ordered regions is smaller, however, in higher-dispersity than in lower-dispersity systems. In contrast to the 5% dispersity system at $H = 2.50$, large regions of locally square order are not found in the 15%

dispersity sample. This result is consistent with earlier observations that dispersity reduces the length scale associated with MRCO [29]. Collectively, our results indicate that these length scales are strongly sensitive to the extent of confinement in polydisperse systems.

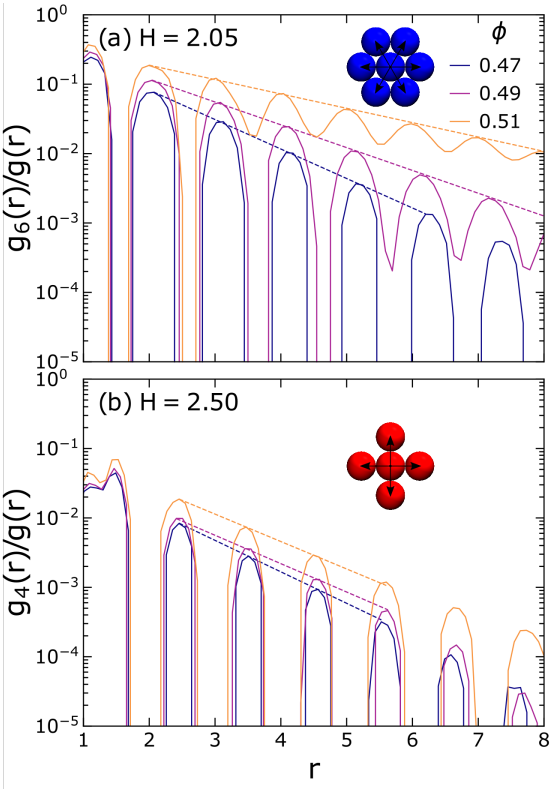

Figure 4. Representative hexatic $g_6(r)/g(r)$ and square $g_4(r)/g(r)$ correlation functions for systems with $s = 0.15$ and volume fractions ϕ denoted in the legend. (a) Hexatic correlation function $g_6(r)/g(r)$ for $H = 2.05$. (b) Square correlation function $g_4(r)/g(r)$ for $H = 2.50$. Dashed lines are error-weighted fits of the peaks of the correlation functions to decaying exponential functions (Eq. 6). The illustration in each panel depicts the type of bond-orientational order characterized by the correlation function.

To extract the characteristic length scales associated with hexatic and square local order, we calculate the correlation functions $g_6(r)/g(r)$ and $g_4(r)/g(r)$, respectively (Fig. 4). The envelope of each correlation function can be fit using a decaying exponential (Eq. 6) to extract static correlation lengths associated with square and hexatic order (ξ_4 and ξ_6, respectively). The hexatic length scale ξ_6 grows steeply with ϕ for $2.00 \leq H \leq 2.34$ and $2.70 \leq H \leq 3.00$, the systems with commensurate packing (Fig. 5(a)). For systems with strongly incommensurate packing ($H = 2.50$ and 2.55), however, ξ_6 is nearly independent of ϕ. For these systems, particles of average size cannot organize into hexagonal layers parallel to the confining walls at these high volume fractions [31, 32]. Thus, hexatic ordering is frustrated by the competition between in-plane and out-of-plane packing within incommensurately-packed systems. In addition, ξ_6 exhibits re-entrance as the wall separation H is increased for all ϕ. This structural re-entrance follows the dynamic re-entrance observed in our simulations (Fig. 1) and in earlier studies [17, 20].

By contrast, the square correlation length ξ_4 does not grow strongly with ϕ for any H (Fig. 5(b)). The prevalence of square ordering increases with ϕ for $H = 2.50$ and $H = 2.55$, but this behavior is not associated with an increase in the static correlation

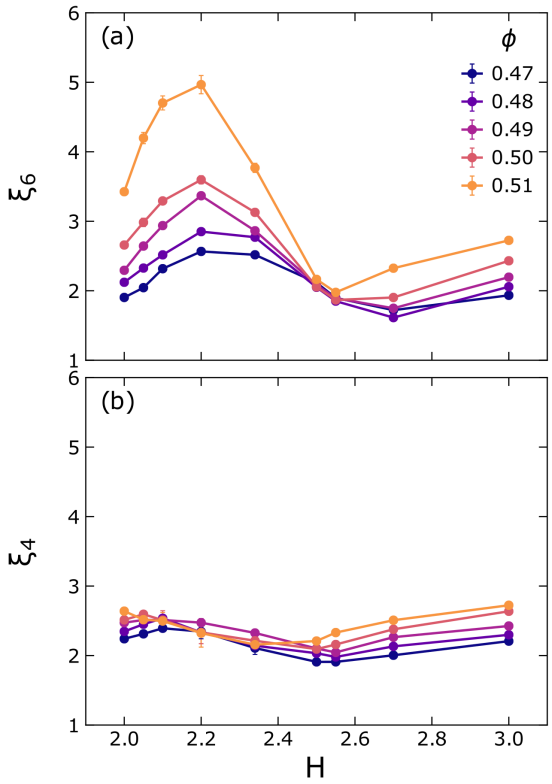

Figure 5. Correlation length scales associated with (a) ξ_6 and (b) ξ_4 for particles within the contact layers adjacent to the walls as a function of H. The systems have polydispersity $s = 0.15$ and volume fractions ϕ indicated in the legend. Error bars reflect uncertainties in ξ_l from fits of the peaks of $g_l(r)/g(r)$ to decaying exponential functions (Eq. 6).

length ξ_4. Instead, it manifests as an increase in the exponential prefactor A (Eq. 6). In the conventional OZ formalism, A is a local analytic function unrelated to the static correlation length [39]. This behavior indicates that square ordering is primarily local. The local nature of square ordering likely arises from its greater susceptibility to frustration [21, 25], which has been attributed to mechanical instabilities associated with this type of order in confined hard-spheres [45].

The relatively small magnitudes of ξ_6 and ξ_4 for $H = 2.50$ compared to the values at other H indicate that square and hexatic ordering compete in these systems. Examination of the local order parameters for $H = 2.50$ provides additional support for this idea. The absence of well-defined hexatic and square regions indicates that no one type of order is dominant and that the development of local crystalline motifs is frustrated (Fig. 3(h)). The relative dominance of square ordering for $H = 2.50$ at $s = 0.05$ (Fig. 3(d)) suggests that increasing polydispersity facilitates competition between domains with different local order, which has been observed for bulk systems [43, 46].

To directly assess the role of hexatic ordering on the slowing of dynamics, we examine the dependence of the in-plane relaxation time τ_{xy} on ξ_6. For wall separations that lead to approximately commensurate packing ($H = 2.00$, 2.34, and 3.00), ξ_6 increases logarithmically with τ_{xy} (Fig. 6). A similar dependence of the relaxation time on the hexatic length scale was also observed in simulations of 2-D polydisperse particle, binary metal, driven granular, and binary spin systems exhibiting MRCO [21, 23, 25]. This behavior is consistent with scaling arguments for the relaxation time derived from

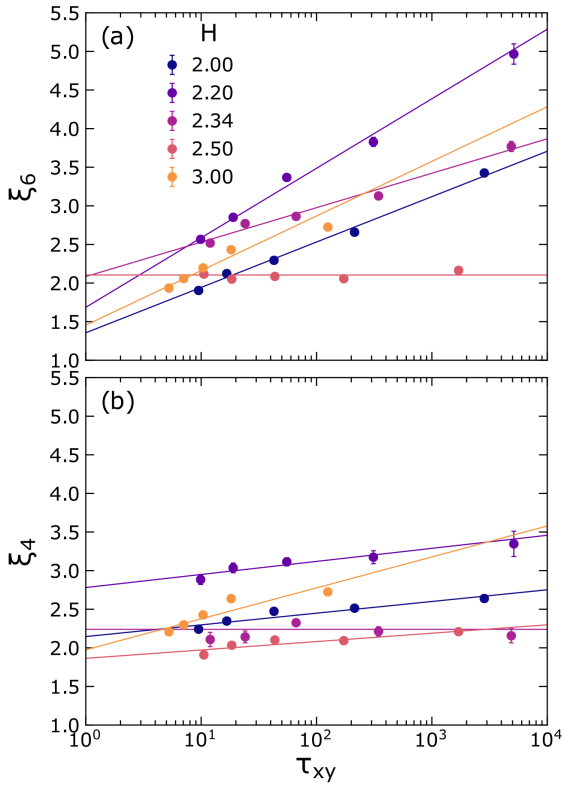

Figure 6. Correlation length scales associated with (a) ξ_6 and (b) ξ_4 for particles within the contact layers adjacent to the walls as a function of the in-plane relaxation time τ_{xy}. The systems have polydispersity $s = 0.15$ and wall separations H indicated in the legend. Solid lines are fits to the relation $\tau_{xy} = B \exp(C\xi_l)$, where B and C are positive constants and ξ_l is either ξ_4 or ξ_6.

2-D random first-order theory (RFOT) [33]. The RFOT framework predicts that, below a threshold temperature (or above a threshold density, for hard spheres), a glassy liquid can be described as a mosaic of distinct domains that rearrange cooperatively and are separated by well-defined interfaces [1, 33]. In this low-temperature (or high-density) regime, the relaxation time increases exponentially with the domain size. For the hexatic ordering in our confined systems, the predicted scaling would imply that $\tau_{xy} = B \exp(C\xi_l)$, where B and C are positive constants, which is consistent with our simulation data. Similar scaling is also predicted by the locally-favored structure model for vitrification of Ref. 34. In addition to ξ_4 and ξ_6, several other structural metrics were also analyzed, but were found to exhibit only weak correlations with τ_{xy} for the systems examined here (see Supporting Information). These comparisons collectively suggest dynamical slowing in quasi-2-D systems with commensurate layering is driven by hexatic ordering.

By contrast, ξ_6 is nearly independent of τ_{xy} for $H = 2.50$, which exhibits incommensurate packing (Fig. 6(a)). For this system, hexatic ordering does not appear to drive dynamical slowing, suggesting a different crystalline symmetry or mechanism is responsible. Because local square order is enhanced in this system (Fig. 3(h)), we also examine the scaling of ξ_4 with τ_{xy}. Interestingly, ξ_4 is smaller for $H = 2.50$ compared to $H = 2.00$, 2.34, and 3.00, which likely occurs due to greater disorder in the incommensurate packing for this wall separation. Nonetheless, we find that ξ_4 does not significantly increase with τ_{xy} for any wall separation (Fig. 6(b)), suggesting square

ordering is not strongly associated with dynamical slowing. Our results show that the relaxation time increases logarithmitically with the static correlation length associated with hexatic MRCO in commensurately-packed systems with $H \lesssim 2.34$. Similar behavior is not observed for the incommensurate system with $H \approx 2.50$. Whether dynamical slowing in this system is associated with a growing static correlation length or a different underlying physical mechanism remains an open question.

4. Conclusions

In this study, we investigated the connection between local structural ordering and the unusual re-entrant dynamics observed for polydisperse hard-sphere liquids confined in small slit pores. At low polydispersity, hexatic and square local order dominate in systems with commensurate and incommensurate packings, respectively. At higher polydispersities, the competition between hexatic, square, and liquid-like order is more pronounced, consistent with the reduction in MRCO observed in unconfined liquids as dispersity is increased.

For commensurate packings with $H \lesssim 2.34$, we found that the static correlation length associated with local hexatic order increased logarithmically with the relaxation time scale, in agreement with the prediction from 2-D random first-order theory. By contrast, square ordering was short-ranged and was not associated with a growing length scale. The short-ranged square ordering and lack of well-defined ordered domains indicated that incommensurately-packed systems were more geometrically frustrated than commensurately-packed systems. For $H = 2.50$, the growth of MRCO was frustrated, yet dynamical slowing with increasing ϕ persisted. Together, these results suggest that a growing static length scale associated with bond orientational order can contribute to dynamical slowing in strongly-confined hard-spheres. Moreover, they show that the influence of bond-orientational order on dynamical slowing may be altered by slight changes in the extent of confinement.

Our analysis revealed a growing length scale associated with hexatic local order for systems with commensurate packing. For the incommensurately-packed, strongly frustrated systems, a growing length scale has yet to be identified. It is of interest to ask whether other dynamic and static length scales [28], such as the dynamical correlation length [8] or point-to-set length scale [47, 48], and/or the structural entropy [29, 49] also exhibit re-entrance that correlates with the dynamics. Further, the connection between local structure and dynamics in polydisperse liquids may be affected by the nature of the particle size distribution (e.g. Gaussian versus Pareto-distributed particle sizes [50, 51]) [38]. Future investigations in these areas are expected to provide additional insight into how the mechanisms for dynamical slowing differ in 2-D, quasi-2-D, and 3-D systems.

Acknowledgements

This work was completed in part with resources provided by the Research Computing Data Core at the University of Houston.

Disclosure statement

No potential conflict of interest was reported by the authors.

Funding

The authors acknowledge support from the Welch Foundation (E-1869 to J.C.C. and E-1882 to J.C.P.) and the National Science Foundation (CBET-1705968).

References

[1] L. Berthier and G. Biroli, Rev. Mod. Phys. **83** (2), 587–645 (2011).
[2] S. Karmakar, C. Dasgupta and S. Sastry, Rep. Prog. Phys. **79** (1), 016601 (2015).
[3] C.A. Angell, Science **267** (5206), 1924–1935 (1995).
[4] P.G. Debenedetti and F.H. Stillinger, Nature **410** (6825), 259–267 (2001).
[5] M.D. Ediger, Annu. Rev. Phys. Chem. **51** (1), 99–128 (2000).
[6] L. Berthier and R.L. Jack, Phys. Rev. E **76** (4), 041509 (2007).
[7] A. Widmer-Cooper and P. Harrowell, J. Non-Cryst. Solids **352** (42-49), 5098–5102 (2006).
[8] N. Lačević, F.W. Starr, T.B. Schrøder and S.C. Glotzer, J. Chem. Phys. **119** (14), 7372–7387 (2003).
[9] L. Berthier, G. Biroli, J.P. Bouchaud, L. Cipelletti, D. El Masri, D. L'Hôte, F. Ladieu and M. Pierno, Science **310** (5755), 1797–1800 (2005).
[10] S. Karmakar, C. Dasgupta and S. Sastry, Proc. Natl. Acad. Sci. U.S.A. **106** (10), 3675–3679 (2009).
[11] H. Löwen, J. Phys. Condens. Matter **13** (24), R415–R432 (2001).
[12] G. Kritikos, N. Vergadou and I.G. Economou, J. Phys. Chem. C **120** (2), 1013–1024 (2016).
[13] C.J. Ellison and J.M. Torkelson, Nat. Mater. **2** (10), 695–700 (2003).
[14] H.B. Eral, D. van den Ende, F. Mugele and M.H.G. Duits, Phys. Rev. E **80** (6), 061403 (2009).
[15] C.R. Nugent, K.V. Edmond, H.N. Patel and E.R. Weeks, Phys. Rev. Lett. **99** (2), 025702 (2007).
[16] S. Lang, V. Boţan, M. Oettel, D. Hajnal, T. Franosch and R. Schilling, Phys. Rev. Lett. **105** (12), 125701 (2010).
[17] S. Mandal, S. Lang, M. Gross, M. Oettel, D. Raabe, T. Franosch and F. Varnik, Nat. Commun. **5**, 4435 (2014).
[18] S. Lang, R. Schilling, V. Krakoviack and T. Franosch, Phys. Rev. E **86** (2), 021502 (2012).
[19] S. Lang, R. Schilling and T. Franosch, J. Stat. Mech.: Theory Exp. **2013** (12), P12007 (2013).
[20] J. Mittal, T.M. Truskett, J.R. Errington and G. Hummer, Phys. Rev. Lett. **100** (14), 145901 (2008).
[21] T. Kawasaki, T. Araki and H. Tanaka, Phys. Rev. Lett. **99** (21), 215701 (2007).
[22] K. Watanabe and H. Tanaka, Phys. Rev. Lett. **100** (15), 158002 (2008).
[23] Y.C. Hu, H. Tanaka and W.H. Wang, Phys. Rev. E **96** (2), 022613 (2017).
[24] U. Gasser, A. Schofield and D.A. Weitz, J. Phys. Condens. Matter **15** (1), S375–S380 (2002).
[25] H. Tanaka, T. Kawasaki, H. Shintani and K. Watanabe, Nat. Mater. **9**, 324–331 (2010).
[26] M. Leocmach and H. Tanaka, Nat. Commun. **3**, 974 (2012).
[27] W.S. Xu, Z.Y. Sun and L.J. An, Phys. Rev. E **86** (4), 041506 (2012).
[28] I. Tah, S. Sengupta, S. Sastry, C. Dasgupta and S. Karmakar, Phys. Rev. Lett. **121** (8), 085703 (2018).

[29] K. Watanabe, T. Kawasaki and H. Tanaka, Nat. Mater. **10**, 512–520 (2011).
[30] P. Pieranski, L. Strzelecki and B. Pansu, Phys. Rev. Lett. **50** (12), 900 (1983).
[31] S. Neser, C. Bechinger, P. Leiderer and T. Palberg, Phys. Rev. Lett **79** (12), 2348 (1997).
[32] A. Fortini and M. Dijkstra, J. Phys. Condens. Matter **18** (28), L371–L378 (2006).
[33] T.R. Kirkpatrick, D. Thirumalai and P.G. Wolynes, Phys. Rev. A **40** (2), 1045–1054 (1989).
[34] H. Tanaka, J. Chem. Phys. **111** (7), 3163–3174 (1999).
[35] E. Zaccarelli, C. Valeriani, E. Sanz, W.C.K. Poon, M.E. Cates and P.N. Pusey, Phys. Rev. Lett. **103**, 135704 (2009).
[36] N.D. Mermin, Phys. Rev. **176** (1), 250 (1968).
[37] J. Russo and H. Tanaka, Proc. Natl. Acad. Sci. U.S.A. **112** (22), 6920–6924 (2015).
[38] L. Berthier, P. Charbonneau, A. Ninarello, M. Ozawa and S. Yaida, Nat. Commun. **10**, 1508 (2019).
[39] M. Campanino, D. Ioffe and Y. Velenik, Probab. Theory Relat. Fields **125** (3), 305–349 (2003).
[40] F. Varnik and T. Franosch, J. Phys. Condens. Matter **28** (13), 133001 (2016).
[41] S. Mandal, S. Lang, V. Boţan and T. Franosch, Soft Matter **13** (36), 6167–6177 (2017).
[42] A.B. Fontecha, H.J. Schöpe, H. König, T. Palberg, R. Messina and H. Löwen, J. Phys. Condens. Matter **17** (31), S2779–S2786 (2005).
[43] M. Fasolo and P. Sollich, Phys. Rev. Lett. **91** (6), 068301 (2003).
[44] H. Tong, P. Tan and N. Xu, Sci. Rep. **5**, 15378 (2015).
[45] K. Nygård, S. Sarman and R. Kjellander, J. Chem. Phys. **141** (9), 094501 (2014).
[46] P. Sollich and N.B. Wilding, Phys. Rev. Lett. **104** (11), 118302 (2010).
[47] G. Biroli, J.P. Bouchaud, A. Cavagna, T.S. Grigera and P. Verrocchio, Nat. Phys. **4** (10), 771–775 (2008).
[48] G.M. Hocky, T.E. Markland and D.R. Reichman, Phys. Rev. Lett. **108** (22), 225506 (2012).
[49] A. Baranyai and D.J. Evans, Phys. Rev. A **40** (7), 3817–3822 (1989).
[50] A. Ninarello, L. Berthier and D. Coslovich, Phys. Rev. X **7** (2), 021039 (2017).
[51] K. Zhang, B. Dice, Y. Liu, J. Schroers, M.D. Shattuck and C.S. O'Hern, J. Chem. Phys. **143** (5), 054501 (2015).